Composites Research

Vol. 31, No. 5, 267-275 (2018)
DOI: http://dx.doi.org/10.7234/composres.2018.31.5.267
ISSN 2288-2103(Print), ISSN 2288-2111(Online)

Paper

The Influence of Carbonization Temperature and KOH Activation Ratio on the Microporosity of N-doped Activated Carbon Materials and Their Supercapacitive Behaviors

Yeong-Rae Son*, Young-Jung Heo*, Eun-A Cho*, Soo-Jin Park*†

ABSTRACT: A facile method for the preparation of nitrogen-doped microporous carbon via the pyrolysis of poly(vinylidene fluoride) (PVDF) using polypyrrole (PPy) as a selective nitrogen source was developed. A PVDF/PPy-800 sample (carbonized at 800°C) with a 1:0.5 ratio of PVDF and PPy exhibited the highest micropore volume. The activated microporous carbon materials obtained from PVDF/PPy-800 prepared at 800°C with KOH possessed a large specific surface area and narrow pore-size distribution. They were characterized using N_2 adsorption at 77 K and argon (Ar) adsorption at 87 K, which allowed for the characterization of the narrow microporosity of the prepared materials due to the absence of interactions between Ar and the sample surface. In addition, the activated microporous carbon material with a KOH/carbon ratio of 2:1 was found to exhibit the largest specific surface area (1296 $m^2 g^{-1}$ in N_2 at 77 K) and microporosity, and a high specific capacitance (122.8 F g^{-1}).

Key Words: Supercapacitor, KOH activation, Microporous carbon, Ar adsorption, Microporosity

1. INTRODUCTION

Electrochemical double-layer capacitors, also known as supercapacitors, are used in a number of industrial applications such as portable electronic devices and hybrid electric vehicles. Supercapacitors can be used to replace conventional batteries and capacitors due to their high specific power, long life cycle, and high dynamic of charge propagation [1,2]. However, the energy density of supercapacitors is smaller than that of secondary/rechargeable batteries. To date, research has therefore focused on enhancing the energy density of supercapacitors with the electrode being a key component in terms of charge storage and delivery, thus playing a crucial role in determining the energy and power densities of supercapacitors [3-5]. Among the various electrode materials used for supercapacitors, carbon materials are the most commonly used due to their low cost, large surface area, good electric conductivity, and excellent chemical stability. For example, porous carbon materials have been widely used as electrode materials in supercapacitors [6,7]; the high specific surface area and pore-size distribution (PSD) of these materials are necessary to achieve a high specific capacitance at the carbon electrode, which is a key requirement for supercapacitors [8,9]. However, the majority of activated carbon materials are not suitable for such applications because of their broad PSD, and so controlling their microstructure to obtain the desired narrow PSD is important [10-13].

For the preparation of the microporous carbon structures, poly(vinylidene fluoride) (PVDF) can be used as the polymer precursor, with simple carbonization yielding the desired structures [14-17]. By this means, Li *et al.* [18] investigated the electrochemical performance of a nitrogen N-enriched carbon sphere and found that high specific capacitance (159 F g^{-1}) was achieved at 0.5 A g^{-1}. This demonstrates that the presence of an N-containing group can improve the surface wettability and reduce the resistance of the carbon sphere [19]. The post-treatment of carbon materials with an N-enriched precursor (e.g. NH_3) is common but disadvantageous in terms of yield and cost [20-22]. The incorporation of heteroatoms such as nitrogen into these carbon structures has been shown to

Received 31 July 2018, received in revised form 27 September 2018, accepted 1 October 2018

*Department of Chemistry, Inha University, Incheon 22212, Korea
*†Department of Chemistry, Inha University, Incheon 22212, Korea, Corresponding author (E-mail: sjpark@inha.ac.kr)

increase their electrochemical performance and suppresses the destruction of the surface structures. For example, doping *via* the carbonization of an N-enriched polymer is a relatively straightforward method for achieving this [23-26]. The use of polypyrrole (PPy) as a nitrogen source has been reported where the nitrogen atoms in the pyrrole rings are readily converted to graphitic N at elevated temperatures [27,18]. The doping of carbon materials with nitrogen has been shown to enhance the electrochemical performance of the materials and has proved to be an effective approach toward increasing capacitance [29].

In terms of the chemical activators for this process, KOH is particularly effective and is the most widely used in the preparation of microporous materials. A key parameter for achieving a high electrochemical performance in an electrode is the choice of an appropriate and narrow PSD. Therefore, activated carbon materials prepared using KOH have a strong potential for application in supercapacitor electrodes due to their high specific surface area and narrow micro-PSD [31,32].

The pore properties of porous materials are usually described in terms of the PSD, which is evaluated by the analysis of N_2 or argon (Ar) adsorption rates. In the past few years, the adsorption of Ar at its boiling temperature (87 K) has been proposed as an alternative adsorptive test to N_2 adsorption for pore size and surface area analysis. Ar analysis is expected to give a more accurate PSD than N_2 analysis because Ar is much less reactive than N_2. In addition, Ar has no dipole or quadrupole moment and Ar adsorption shows a much more straightforward correlation among pressure, micropore filling, and pore size [33].

Herein, we report studies into the synthesis of an N-doped porous carbon material through the pyrolysis of PPy as the nitrogen source and using PVDF as the polymer precursor. The resulting N-doped porous carbon was treated with KOH to obtain the activated carbon materials with a microporous structure and narrow PSD. The microporosity of the prepared samples was estimated by the adsorption of both Ar and N_2. Finally, we systematically investigated the electrochemical performance of the resulting materials, especially focusing on the influence of microporosity of N-doped activated carbon materials.

2. EXPERIMENTAL

2.1 Materials and methods

PVDF and PPy (both from Aldrich) were used as the precursors for the preparation of the N-doped microporous carbon materials.

A mixture of PVDF and PPy (with a weight ratio of 1.0:0.5) was placed in a tubular furnace with an alumina tube to carry out the stabilization and carbonization steps. The mixture was stabilized at 200°C for 2 h (hour), then carbonization was carried out at either 700, 750, 800, 850, or 900°C for 1 h under N_2 with a heating rate of 3°C min^{-1} and an N_2 flow rate of 200 mL min^{-1}. The porous carbon materials prepared at these specified temperatures were named PVDF/PPy-700, 750, 800, 850, and 900, with the number reflecting the carbonization temperature.

Following carbonization, PVDF/PPy-800 and KOH were mixed in weight ratios of 1:1, 1:2, and 1:4, and were activated at 800°C using N_2 with a heating rate of 2°C min^{-1} and kept for 1 h. The resulting materials were washed with a 1.7 M HCl solution and distilled water to remove residual KOH, and were subsequently dried at 120°C for 12 h. From here on, the PVDF/PPy-800 is referred to as microporous carbon (MC), while the activated microporous carbon is referred to as A-MCχ, where χ denotes the KOH/MC ratio.

2.2 Measurements

The elemental composition of the samples as a function of surface treatment was investigated using X-ray photoelectron spectroscopy (XPS) on an ESCALAB Mk-II spectrometer (VG Scientific Co., UK) equipped with a monochromatic Al Kα radiation source. The porous texture of the prepared samples was analyzed at 77 K for N_2 adsorption and 87 K for Ar adsorption using a gas adsorption analyzer (BELSORP, BEL JAPAN). The specific surface area was determined by applying the Brunauer–Emmett–Teller (BET) equation at a relative pressure P/P_0 of 0.995. In addition, the micropore volume and PSD were calculated using the Dubinin–Radushkevich (DR) equation. The electrochemical behavior of the working electrode was analyzed using a three-electrode configuration in a 6 M KOH electrolyte with a Pt wire reference electrode and an Ag/AgCl counter electrode. The working electrode was prepared using 80 wt.% (weight%) of prepared activated MCs, 10 wt.% carbon black conductive agent, and 10 wt.% PVDF binding material. Cyclic voltammetry and galvanostatic charge-discharge cycling were employed in the evaluation of the electrochemical behavior of each sample using an Ivium-Stat instrument. The cyclic voltammetry measurements were carried out at scan rates of 10–100 mV s^{-1} in a potential range of −0.7 to 0.1 V. Galvanostatic charge/discharge curves were obtained at current densities from 0.5–2 A g^{-1} in a potential range of −1 to 0 V. The specific capacitance of the products was estimated according to

$$C = \frac{I \times \Delta t}{\Delta V \times m} \quad (1)$$

where C is the capacitance of the cell, I is the discharge current, Δt is the discharge time, ΔV is the potential range, and m is the mass of active material on the electrode.

3. RESULTS AND DISCUSSION

Table 1 lists the textural properties for the pore structures of the PVDF/PPy samples. In addition, the N_2 adsorption/desorption isotherms and micro-PSD of the PVDF/PPy sam-

Table 1. The textural properties of the microporous carbons prepared at different temperatures.

	S_{BET} [a]	V_{total} [b]	V_{meso} [c]	V_{micro} [d]	F_{micro} [d]
PVDF/PPy 700	346	0.2565	0.1498	0.1067	41.60
PVDF/PPy 750	375	0.3045	0.1920	0.1125	36.95
PVDF/PPy 800	551	0.3444	0.1552	0.1892	54.94
PVDF/PPy 850	568	0.3508	0.1690	0.1818	51.82
PVDF/PPy 900	581	0.3658	0.1885	0.1773	49.03

The measurements were conducted with N_2 at 77 K.
[a] Specific surface area [$m^2 g^{-1}$]
[b] Total pore volume [$cm^3 g^{-1}$]
[c] Mesopore volume [$cm^3 g^{-1}$]
[d] Micropore volume [$cm^3 g^{-1}$]
[e] (Micropore volume/total pore volume) × 100(%)

ples are shown in Fig. 1a and b, respectively. As can be seen, the pore structure depended on the heat treatment temperature since the specific surface area increased with increasing temperature up to 900°C, although a decrease in micropore volume was also observed at this temperature. PVDF/PPy-900 was found to have a large specific surface area of 581 $m^2 g^{-1}$, while PVDF/PPy-800 exhibited the higher micropore volume of 0.1892 $cm^3 g^{-1}$ than other PVDF/PPy samples due to the collapse of the micropores at high carbonization temperatures (i.e. 850 and 900°C). In addition, the specific surface area and micropore volume were enhanced by a pore development mechanism based on the complete release of hydrogen fluoride (HF) from the carbon chains of PVDF during treatment. Furthermore, the results show that the carbonization temperature can be used to control the porous structure, thus indicating the easy transfer and good accessibility of the electrolyte ions in supercapacitor electrodes. Thus, for the KOH activation step, PVDF/PPy-800 was prepared as the precursor by carbonization at the optimum temperature, i.e. 800°C.

3.1 The morphologies of the A-MC materials

As previously mentioned, MCs tend to generate pores randomly to release fluoride ions in the form of HF. Fig. 2 shows SEM images of representative MC and A-MC materials. As can be seen, the structure of MC resembles tree branches, and following KOH activation, a similar type of structure but with a slightly more complex morphology due to the harsh KOH activation process can be observed in the SEM image of A-MC 2. The porosity of these samples was therefore based on an ion reservoir offering short pathways for ions through the electrode.

3.2 The characterization of the A-MC materials

The elemental components of the A-MC materials are listed in descending order of N content in Table 2. The nitrogen content determined by the XPS analysis was found to be 2.61, 2.12, 1.27, and 0.80 wt.% for MC, A-MC 1, A-MC 2, and AM-C 4, respectively. This decrease in nitrogen content with increasing KOH ratio was due to the etching effect of the KOH activation. In contrast, following KOH activation, the oxygen content increased significantly, with values more than doubling for the A-MCs compared to the MC. The KOH activation process resulted in redox reactions through following redox reactions:

$$2KOH \rightarrow K_2O + H_2O \quad (1)$$

$$C + H_2O \rightarrow CO + H_2 \quad (2)$$

$$CO + H_2O \rightarrow CO_2 + H_2 \quad (3)$$

$$CO_2 + K_2O \rightarrow K_2CO_3 \quad (4)$$

$$K_2O + H_2 \rightarrow 2K + H_2O \quad (5)$$

$$K_2O + C \rightarrow 2K + CO \quad (6)$$

Reactions (1)-(4) and (5) and (6) are activation mechanisms at temperatures below and above 700°C, respectively. According to this reaction mechanism, carbon and nitrogen in the activated carbon lattice are oxidized by KOH and oxygen functional groups are introduced, thus the oxygen content is increased [34,35].

Fig. 3 presents the N1s XPS spectra of MC and the A-MCs.

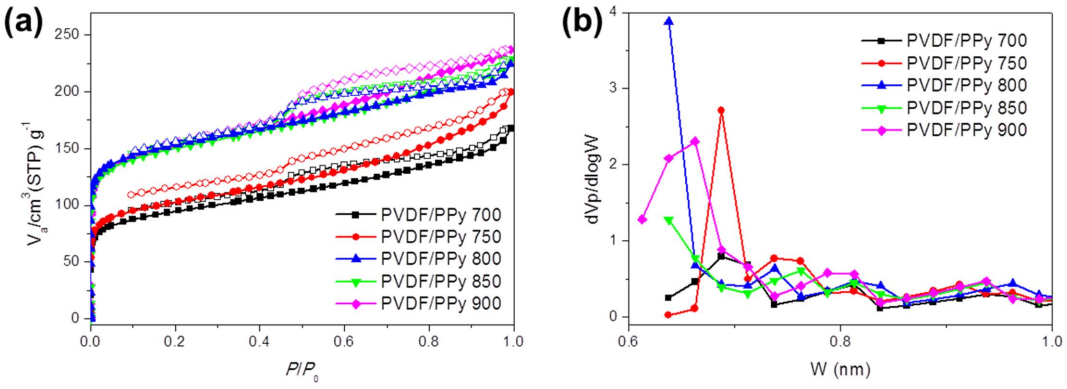

Fig. 1. (a) Adsorption/desorption isotherms and (b) micropore size distribution of the microporous carbons prepared at different temperatures. The measurements were conducted in N_2 at 77 K

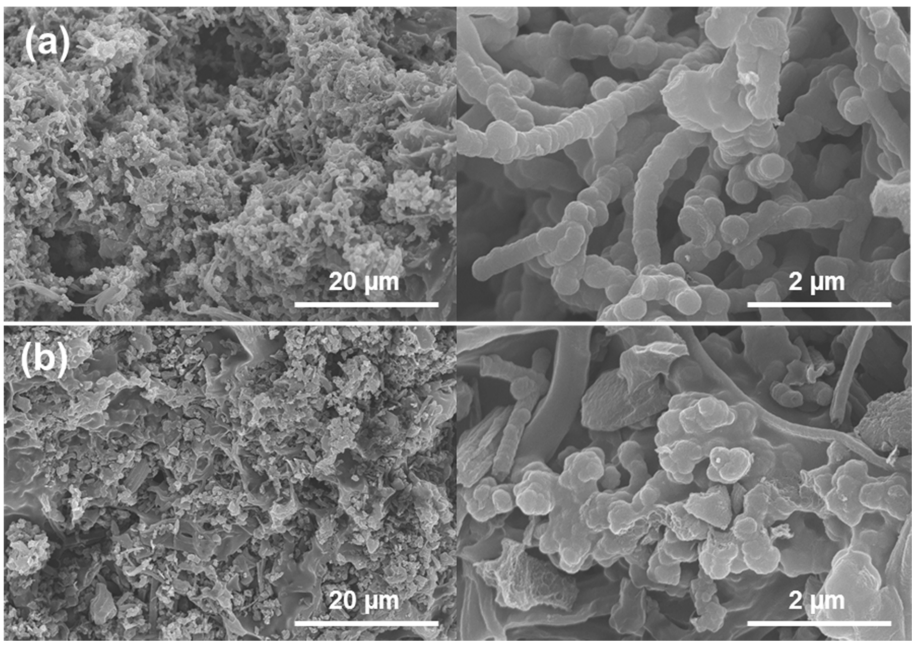

Fig. 2. SEM micrographs of (a) MC and (b) A-MC 2

Table 2. The elemental components of MC and the A-MCs (wt.%)

	C	O	N	F
MC	90.25	6.67	2.61	0.46
A-MC 1	76.82	20.53	2.12	0.48
A-MC 2	77.33	21.11	1.27	0.30
A-MC 4	84.67	14.02	0.80	0.52

To evaluate the nitrogen binding state in the samples, curve fitting was carried out using XPSpeak 4.1 software. The fitting parameters, background type, full width at half maximum (FWHM), and %Lorentzian-Gaussian (%L-G), were set to Shirley-type, 1.4 eV, and 50%, respectively. From the deconvoluted N1s XPS spectra, it was found that MC and the A-MCs consisted mainly of 3–5 N-containing functional groups, namely pyridinic N (N-6, 398 eV), nitrile N (Nt, 399.1 eV), pyrrolic N (N-5, 400.4 eV), quaternary N (N-Q, 401.3 eV), and nitrogen oxide (NOx-N, 402.5–403 eV) peaks, where the pyrrolic N-5 and pyridinic N-6 were located at the edges of the graphene structure.

These nitrogen components were considered to have affected the pseudo-capacitance of the materials. Furthermore, each N-Q atom was bonded to three C atoms in the central position of the graphene structure and together were responsible for generating a positive charge, thus they had an effect on electron transfer. When the MC was activated by KOH, the percentage of the N-5 state was decreased and the Nt state arose. Meanwhile, the fraction of N-Q state that affects pseudo-capacitance varies with the KOH ratio. The N-Q state of A-MC 1 was analyzed to be almost non-existent. On the other hand, the N-Q state of A-MC 2 and A-MC 4 increased with decreasing N-6 state. However, it was confirmed that the N-Q state of A-MC 4 was fractionally less than that of A-MC 2, which led to the reduction in pseudo-capacitance. The atomic percentages of nitrogen for the various chemical states of the samples studied can be found in Table 3.

Table 3. The atomic percentages of the various chemical states of nitrogen in MC and the A-MCs (%).

	N-6	Nt	N-5	N-Q	NOx-O
MC	42.7	-	41.9	8.8	6.6
A-MC 1	47.4	34.7	17.8	-	-
A-MC 2	22.4	35.1	17.6	14.0	11.0
A-MC 4	14.0	45.5	21.6	6.1	12.8

3.3 The textural properties of the A-MC materials

For investigation of the textural properties of the A-MC materials, each was prepared using the PVDF/PPy-800 precursor as it possessed the largest microporous volumes of all of the A-MCs reported herein. The isotherms of N_2 adsorption at 77 K for MC and the A-MCs are shown in Fig. 4a, and detailed texture analyses with the N_2 adsorption isotherms are given in Table 4. In addition, Fig. 4b shows the micro-PSDs at 77 K. According to IUPAC classification, the isotherms of these samples can be classified as type 1 isotherms; i.e. adsorption is limited to a single monolayer of adsorbate at the adsorbent surface. Following KOH activation, the specific surface areas of the A-MCs increased significantly due to the formation of micropores. A-MC 2 was found to have the largest specific surface area (1296 $m^2 g^{-1}$) and the largest total pore volume (0.6264 $cm^3 g^{-1}$) of all of the samples studied. The BET values

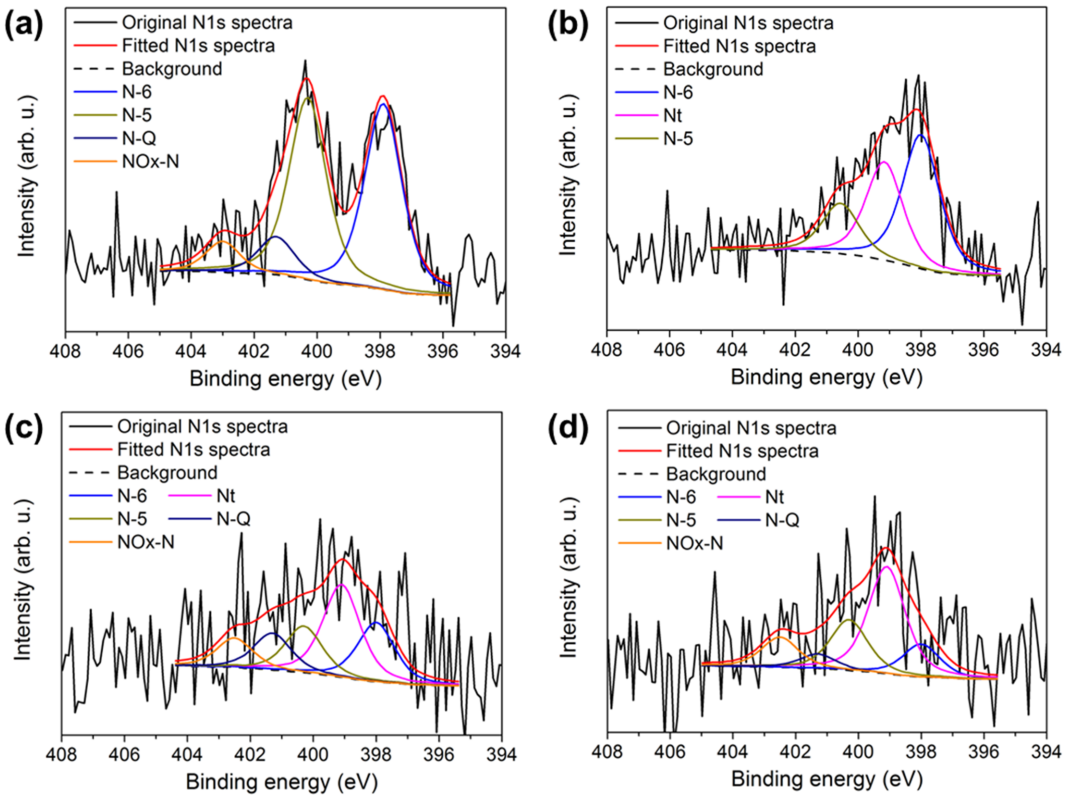

Fig. 3. High-resolution XPS N1s spectra of (a) MC, (b) A-MC 1, (c) A-MC 2, and (d) A-MC 4

Table 4. The textural properties of MC and the A-MCs measured with N_2 at 77 K

	S_{BET} [a]	V_{total} [b]	V_{micro} [d]	D_{mean} [d]
MC	551	0.3444	0.1892	0.64
A-MC 1	1269	0.6186	0.4638	0.69
A-MC 2	1296	0.6264	0.4892	0.64
A-MC 4	1273	0.5995	0.4711	0.69

[a] Specific surface area [$m^2 g^{-1}$]
[b] Total pore volume [$cm^3 g^{-1}$]
[c] Micropore volume [$cm^3 g^{-1}$]
[d] Mean micropore diameter [nm]

and pore-volume increased with an increase in the MC/KOH mixture ratio, although both factors decreased in the case of A-MC 4 due to the collapse of the micropores due to over-activation.

The electrochemical performance of supercapacitors is known to be dependent on the microporosity of the electrode materials because of the size of the hydrated ions in an aqueous electrolyte. A moderate pore size of < 2 nm is required to maximize the ease of mobility and insertion of electrolyte ions into the electrode micropores. In our studies, we observed that the mean micropore diameter decreased with KOH activation, with the A-MCs having a narrow PSD of approximately 0.6–

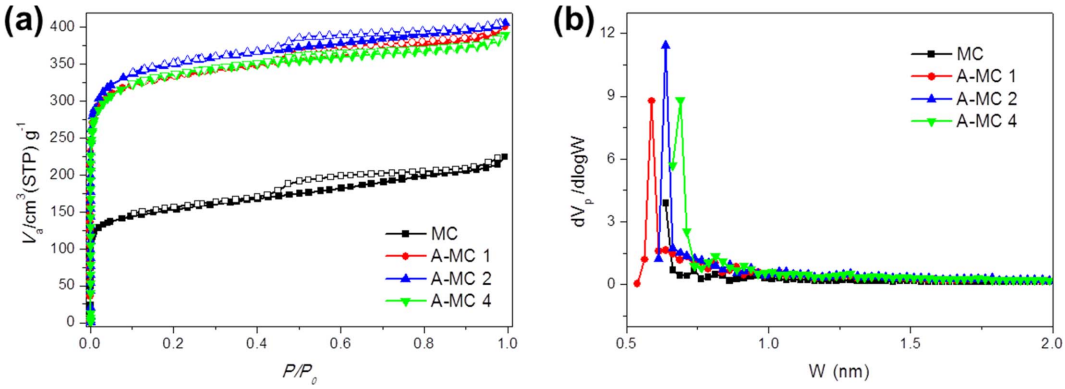

Fig. 4. (a) Adsorption/desorption isotherms and (b) micropore size distribution of the A-MCs measured with N_2 at 77 K

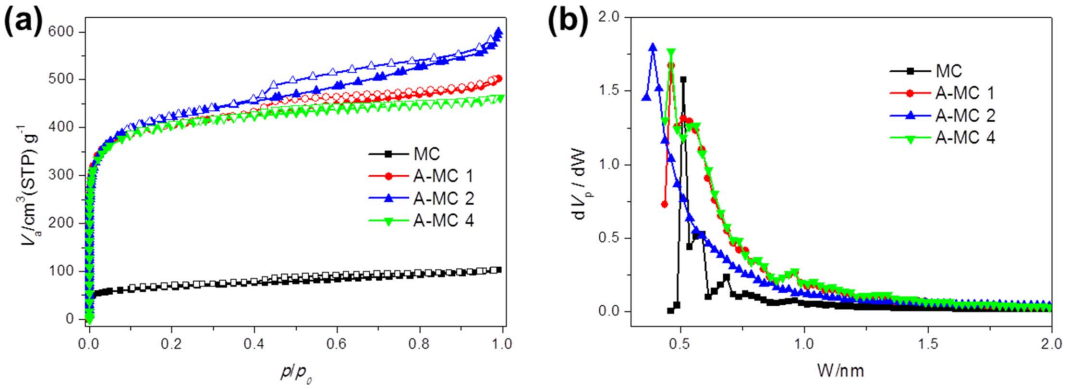

Fig. 5. (a) Adsorption/desorption isotherms and (b) micropore size distribution of the A-MCs measured with Ar at 87 K

Table 5. The textural properties of MC and the A-MCs measured with Ar at 87 K

	S_{BET} [a]	V_{total} [b]	V_{micro} [d]	D_{mean} [d]
MC	383	0.2323	0.1471	0.51
A-MC 1	1358	0.6378	0.5159	0.46
A-MC 2	1389	0.7507	0.5551	0.39
A-MC 4	1335	0.5887	0.5429	0.46

[a] Specific surface area [$m^2 g^{-1}$]
[b] Total pore volume [$cm^3 g^{-1}$]
[c] Micropore volume [$cm^3 g^{-1}$]
[d] Mean micropore diameter [nm]

0.7 nm. As a typical example of the samples studied, A-MC 2 exhibited a large pore volume of 0.6264 $cm^3 g^{-1}$, with the micropores mainly contributing to the total pore volume. These characteristics appear to have resulted from the development of the original pore system during KOH activation, and they are critical for determining the specific capacitance of a supercapacitor.

Fig. 5a and b show the Ar adsorption isotherms and micropore size distribution at 87 K and Table 5 reports the textural properties. It has been previously reported that higher relative pressures are required to fill the pores by Ar adsorption compared to N_2 due to the specific quadrupole interactions of nitrogen with the carbon surface functional groups. The textural properties of the materials were found to increase in the Ar adsorption isotherm at 87 K compared to the N_2 adsorption isotherm at 77 K. In addition, the BET values and total pore volumes of the A-MCs increased from 551 to 383 $m^2 g^{-1}$ whereas those of the MC decreased from 0.3444 to 0.2323 $cm^3 g^{-1}$. It is therefore clear that Ar adsorption is more sensitive than N_2 adsorption toward smaller pores, such as the micropores on our A-MC materials, due to the respective molecular dimensions and weaker effective adsorption potentials.

3.4 The electrochemical performance of the A-MC materials

The electrochemical performances of MC and the A-MCs were evaluated using a 6 M KOH electrolyte solution and a three-electrode system. Fig. 6a shows the cyclic voltammetry (CV) curves of the samples studied at a scan rate of 20 mV s^{-1}. All of the CV curves displayed a quasi-rectangular shape, indicating the coexistence of good accessibility of the electrolyte ions into the active surface area and the great electrochemical behavior of both the MC and the A-MCs; the largest CV curve was observed for A-MC 2. Fig. 6b shows the galvanostatic charge/discharge curves of samples at a current density of 1 A g^{-1} in 6 M KOH solution (also see Table 6), in which the curves all exhibited a triangular shape. In addition, it can be seen that the specific capacitances of the A-MC 1 and A-MC 2 electrodes increased from 47.7 F g^{-1} (for MC) to 85.1 and 122.8 F g^{-1}, respectively, but decreased to 80.9 F g^{-1} for A-MC 4. This result demonstrates that the electrolyte ions quickly diffused and were transported into the samples' pores. Overall, A-MC 2 possessing the largest micropore volume (0.4892 $cm^3 g^{-1}$) and a narrow PSD (the average micropore size diameters was 0.69 nm) showed the highest specific capacitance. Furthermore, it was found that the synergistic effect of low fluorine content and nitrogen functional groups (mainly N-Q) in A-MC 2 affected the diffusion of electrolyte ions. Consequently, the increased specific capacitance of A-MC 2 is attributed to these factors. In Fig. 6c, the CV curves of A-MC 2 with a range of scan rates can be seen. The CV curve at the highest scan rate appeared as a distorted rectangular shape when compared to the lower scan rates for which the CV curves retained their rectangular shape, indicating that the chemical reactivity between the electrode and the electrolyte interface decreased. Therefore, the CV curves of A-MC 2 appear to have been influenced by pore structure, which demonstrates the facile ion mobility through the chemical reactivity between the nitrogen groups in A-MC 2 and the electrolyte ions. As shown in Fig. 6d, the charge/discharge curves of A-MC 2 over a range of current densities were also measured. It was found that the specific capacitance decreased when the current density was increased from 0.5 to 2 A g^{-1}, which demonstrates that A-MC 2 is more stable at lower current densities. Therefore, it can be concluded that A-MC 2

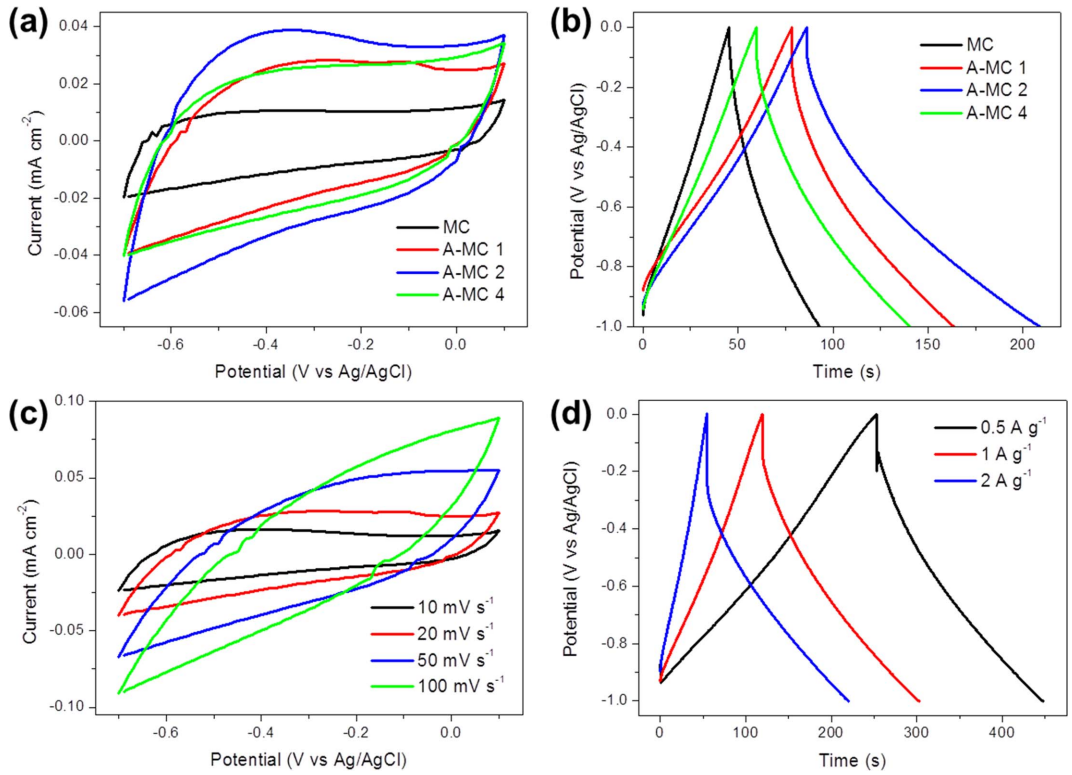

Fig. 6. (a) Cyclic voltammetry curves and (b) galvanostatic charge/discharge behavior of MC and the A-MCs determined at 20 mV s^{-1} and at 1 A g^{-1}, respectively. (c) Cyclic voltammetry curves and (d) galvanostatic charge/discharge behavior of A-MC 2 at various scan rates and current densities

Table 6. The specific capacitance of MC and the A-MCs determined at a current density of 1 A g^{-1}

	MC	A-MC 1	A-MC 2	A-MC 4
Specific capacitance (F g^{-1})	47.7	85.1	122.8	80.9

exhibited a good electrochemical performance due to a high specific surface area and microporous volume resulting from the optimized KOH treatment ratio. The effects of KOH activation were reflected in the pore structure and specific surface area, thus resulting in the improved specific capacitance of the electrode materials.

4. CONCLUSIONS

N-doped A-MC materials were successfully prepared in a two-step process: (1) the carbonization of PVDF/PPy and (2) the KOH activation of the resulting N-doped carbon. It was found out that the samples exhibited higher specific surface areas and micropore volumes along with a uniform PSD following KOH activation. The gas adsorption and electrochemical properties of the MC and A-MCs were influenced by both nitrogen content and micropore structure. A-MC 2 (with a KOH/carbon ratio of 2:1) was found to exhibit excellent specific surface area, micropore volume, and specific capacitance. Our results demonstrate that Ar adsorption was favored over N_2 adsorption in the case of microporosity as Ar is smaller and less reactive than N_2. In addition, we found that the microporosity also affects the electrochemical performance of the supercapacitor.

ACKNOWLEDGEMENTS

This research was supported by the Leading Human Resource Training Program of Regional Neo industry through the National Research Foundation of Korea (NRF) and funded by the Ministry of Science, ICT and Future Planning (NRF-2016H1D5A1909732). This work was also supported by the Technology Innovation Program (or Industrial Strategic Technology Development Program) (10080293, Development of carbon-based non-phenolic electrode materials with 3,000 m^2 g^{-1} grade surface area for energy storage device) funded by the Ministry of Trade, Industry & Energy (MOTIE, Korea).

REFERENCES

1. Xu, B., Hou, S., Zhang, F., Cao, G., Chu, M., and Yang, Y., "Nitrogen-doped Mesoporous Carbon Derived from Biopolymer as Electrode Material for Supercapacitors," *Journal of Elec-*

troanalytical Chemistry, Vol. 712, 2014, pp. 146–150.
2. Lezanska, M., Olejniczak, A., Pacula, A., Szymanski, G., and Wloch, J., "The Influence of Microporosity Creation in Highly Mesoporous N-containing Carbons Obtained from Chitosan on Their Catalytic and Electrochemical Properties," *Catalysis Today*, Vol. 277, 2014, pp. 223–232.
3. Su, F., Zeng, J., Yu, Y., Lv, L., Lee, J.Y., and Zhao, X.S., "Template Synthesis of Microporous Carbon for Direct Methanol Fuel Cell Application," *Carbon*, Vol. 43, 2005, pp. 2366–2373.
4. Frackowiak, E., and Beguin, F., "Carbon Materials for the Electrochemical Storage of Energy in Capacitors," *Carbon*, Vol. 39, 2001, pp. 937–950.
5. Ma, C., Song, Y., Shi, J., Zhang, D., Zhai, X., Zhong, M., Guo, Q., and Liu, L., "Preparation and One-step Activation of Microporous Carbon Nanofibers for Use as Supercapacitor Electrodes," *Carbon*, Vol. 51, 2013, pp. 290–300.
6. Lota, G., Lota, K., and Frackowiak, E., "Nanotubes Based Composites Rich in Nitrogen for Supercapacitor Application," *Electrochemistry Communications*, Vol. 9, 2007, pp. 1828–1832.
7. Pan, Y., Mei, Z., Yang, Z., Zhang, W., Pei, B., and Yao, H., "Facile Synthesis of Mesoporous MnO2/C Spheres for Supercapacitor Electrodes," *Chemical Engineering Journal*, Vol. 242, 2014, pp. 397–403.
8. Guo, P., Gi, Y., Lei, Z., Cui, Y., and Zhao, X.S., "Preparation of Sucrose-based Microporous Carbons and Their Application as Electrode Materials for Supercapacitors," *Microporous and Mesoporous Materials*, Vol. 156, 2012, pp. 176–180.
9. Chen, T., and Dai, L., "Carbon Nanomaterials for High-performance Supercapacitors," *Materials Today*, Vol. 16, 2013, pp. 272–280.
10. Ma, C., Li, Y., Shi, J., Song, Y., and Liu, L., "High-performance Supercapacitor Electrodes Based on Porous Flexible Carbon Nanofiber Paper Treated by Surface Chemical Etching," *Chemical Engineering Journal*, Vol. 249, 2014, pp. 216–225.
11. Chen, J., Jia, C., and Wan, Z., "Novel Hybrid Nanocomposite Based on Poly(3,4-ethylenedioxythiophene)/multiwalled Carbon Nanotubes/graphene as Electrode Material for Supercapacitor," *Synthetic Metals*, Vol. 189, 2014, pp. 69–76.
12. Lee, J.H., Kim, I.J., and Park, S.J., "Preparation and Electrochemical Behaviors of Styrene–acrylonitrile-based Porous Carbon Electrodes," *Electrochimica Acta*, Vol. 113, 2013, pp. 23–28.
13. Kitajima, M., Sato, M., and Nichide, H., "Preparation of Flat Porous Carbon Films from Paper-thin Wood Shavings and Control of their Mechanical, Electrical and Magnetic Properties," *Carbon*, Vol. 61, 2013, pp. 260–269.
14. Kim, K.S., and Park, S.J., "Influence of Multi-walled Carbon Nanotubes on the Electrochemical Performance of Graphene Nanocomposites for Supercapacitor Electrodes," *Electrochimica Acta*, Vol. 56, 2011, pp. 1629–1635.
15. Kim, K.S., and Park, S.J., "Synthesis and High Electrochemical Capacitance of N-doped Microporous Carbon/carbon Nanotubes for Supercapacitor," *Journal of Electroanalytical Chemistry*, 673, 2012, pp. 58–64.
16. Swietlik, U., Grzyb, B., Torchala, K., Grylewicz, G., and Machnikowski, J., "High Temperature Ammonia Treatment of Pitch Particulates and Fibers for Nitrogen Enriched Microporous Carbons," *Fuel Processing Technology*, Vol. 119, 2014, pp. 211–217.
17. Kim, Y.H., and Park, S.J., "Roles of Nanosized Fe3O4 on Supercapacitive Properties of Carbon Nanotubes," *Current Applied Physics*, Vol. 11, 2011, pp. 462–466.
18. Li, W., Chen, D., Li, Z., Shi, Y., Wan, Y., Wang, G., Jiang, Z., and Zhao, D., "Nitrogen-containing Carbon Spheres with very Large Uniform Mesopores: The Superior Electrode Materials for EDLC in Organic Electrolyte," *Carbon*, Vol. 45, 2007, pp. 1757–1763.
19. Wang, Z., Xiong, X., Qie, L., and Huang, Y., "High-performance Lithium Storage in Nitrogen-enriched Carbon Nanofiber Webs Derived from Polypyrrole," *Electrochimica Acta*, Vol. 106, 2013, pp. 320–326.
20. Lin, Z., Waller, G.H., Liu, Y., Liu, M., and Wong, C.P., "3D Nitrogen-doped Graphene Prepared by Pyrolysis of Graphene Oxide with Polypyrrole for Electrocatalysis of Oxygen Reduction Reaction," *Nano Energy*, Vol. 2, 2013, pp. 241–248.
21. Jagiello, J., and Betz, W., "Characterization of Pore Structure of Carbon Molecular Sieves Using DFT Analysis of Ar and H2 Adsorption Data," *Microporous and Mesoporous Materials*, Vol. 108, 2008, pp. 117–122.
22. Meng, L.Y., and Park, S.J., "Effect of Heat Treatment on CO2 Adsorption of KOH-activated Graphite Nanofibers," *Journal of Colloid and Interface Science*, Vol. 352, 2010, pp. 498–503.
23. Jagiello, J., and Thommes, M., "Comparison of DFT Characterization Methods Based on N2, Ar, CO2, and H2 Adsorption applied to Carbons with Various Pore Size Distributions," *Carbon*, Vol. 42, 2004, pp. 1227–1232.
24. Silvestre-Albero, J., Silvestre-Albero, A., Rodriguez-Reinoso, F., and Thommes, M., "Physical Characterization of Activated Carbons with Narrow Microporosity by Nitrogen (77.4K), Carbon Dioxide (273K) and Argon (87.3K) Adsorption in Combination with Immersion Calorimetry," *Carbon*, Vol. 50, 2012, pp. 3128–3133.
25. Xiao, Y., Long, C., Zheng, M.T., Dong, H.W., Lei, B.F., Zhang, H.R., and Liu, Y.L., "High-Capacity Porous Carbons Prepared by KOH Activation of Activated Carbon for Supercapacitors," *Chinese Chemical Letters*, Vol. 25, 2014, pp. 865–868.
26. Kierzek, K., Frackowiak, E., Lota, G., Gryglewicz, G., and Machnikowski, J., "Electrochemical Capacitors Based on Highly Porous Carbons Prepared by KOH Activation," *Electrochimica Acta*, Vol. 49, 2004, pp. 515–523.
27. Daguerre, E., Guillot, A., and Py, X., "Microporosity of Activated Carbons Produced from Heat-treated and Fractionated Pitches," *Carbon*, Vol. 38, 2000, pp. 59–64.
28. Kim, S., and Park, S.J., "Effects of Chemical Treatment of Carbon Supports on Electrochemical Behaviors for Platinum Catalysts of Fuel Cells," *Journal of Power Sources*, Vol. 159, 2006, pp. 42–45.
29. Nguyen, T.X., and Bhatia, S.K., "Characterization of Activated Carbon Fibers Using Argon Adsorption," *Carbon*, Vol. 43, 2005, pp. 775–785.
30. Silvestre-Albero, A., Silvestre-Aebero, J., Martinez-Excandell,

M., Futamura, R., Itoh, T., Kaneko, K., and Rodriquez-Reinoso, F., "Non-porous Reference Carbon for N2 (77.4K) and Ar (87.3K) Adsorption," *Carbon*, Vol. 66, 2014, pp. 699–704.

31. Song, Y., Hu, S., Dong, X., Wang, Y., Wang, C., and Xia, Y., "A Nitrogen-doped Hierarchical Mesoporous/Microporous Carbon for Supercapacitors," *Electrochimica Acta*, Vol. 146, 2014, pp. 485–494.
32. Im, J.S., Lee, Y.S., and Park, S.J., "Preparation and Characteristics of Electrospun Activated Carbon Materials having Meso- And Macropores," *Journal of Colloid and Interface Science*, Vol. 314, 2007, pp. 32–37.
33. Cho, E.A., Lee, S.Y., and Park, S.J., "Effect of Microporosity on Nitrogen-doped Microporous Carbons for Electrode of Supercapacitor," *Carbon Letters*, Vol. 15, 2014, pp. 210–213.
34. Raymundo-Piñero, E., Azaïs, P., Cacciaguerra, T., Cazorla-Amorós, D., Linares-Solano, A., and Béguin, F., "KOH and NaOH Activation Mechanisms of Multiwalled Carbon Nanotubes with Different Structural Organisation," *Carbon*, Vol. 43, 2005, pp. 786–795.
35. Zhou, M., Pu, F., Wang, Z., and Guan, S., "Nitrogen-doped Porous Carbons Through KOH Activation with Superior Performance in Supercapacitors," *Carbon*, Vol. 68, 2014, pp. 185–194.